

Supporting Information

Thermal conduction-induced crystallization and achieving high efficiency in HTM-free carbon-based CsPbI₂Br solar cells by regulating the dipole moment of aliphatic amine acetate additives

Xinlong Zhang^a, Jincheng Huang^{a*}, Hengzhi Zuo^a, Yuanfang Zhang^a, Yuhang Guo^a,
Yifei Shi^b, Jianlin Chen^a, Guijun Li^c, Wei Li^a, Zhuoyin Peng^{a*}

^a Key Laboratory of Efficient & Clean Energy Utilization, School of Energy and Power Engineering, Changsha University of Science and Technology, Changsha 410111, P. R. China

^b School of Electrical and Information Engineering, Changsha University of Science and Technology, Changsha 410114, P. R. China

^c Key Laboratory of Optoelectronic Devices and Systems of Ministry of Education and Guangdong Province, College of Physics and Optoelectronic Engineering, Shenzhen University, Shenzhen 518060, P. R. China

***Corresponding authors**

E-mail addresses: hjc641@163.com (J. Huang), joeypengzy@outlook.com (Z. Peng)

1. Figure section

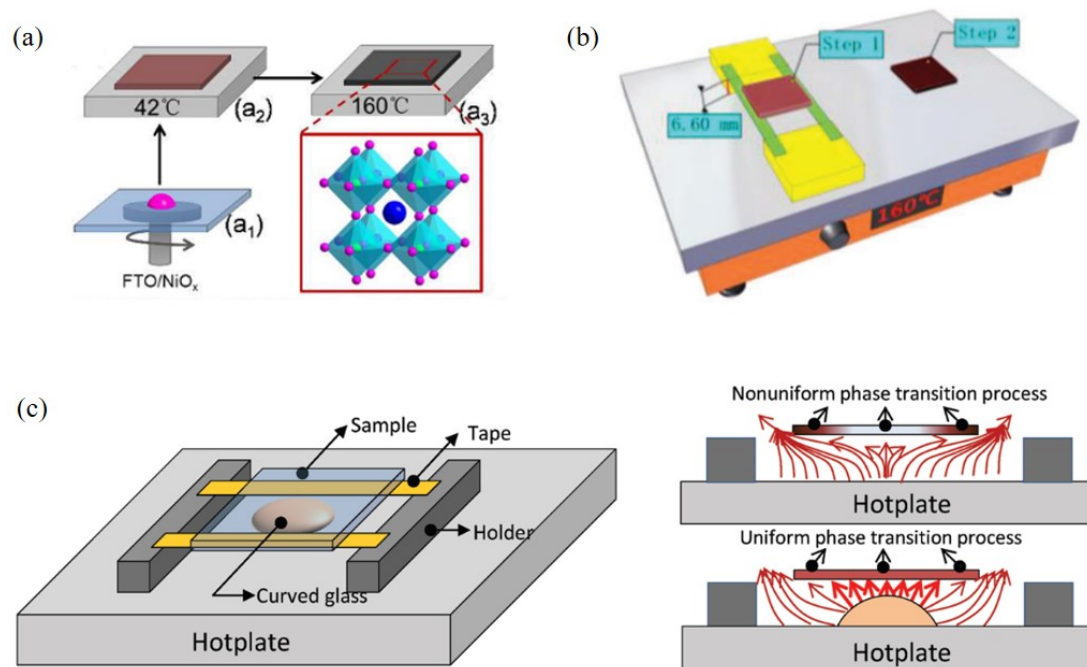


Figure S1. Correlated annealing pattern evolution diagram[1-3].

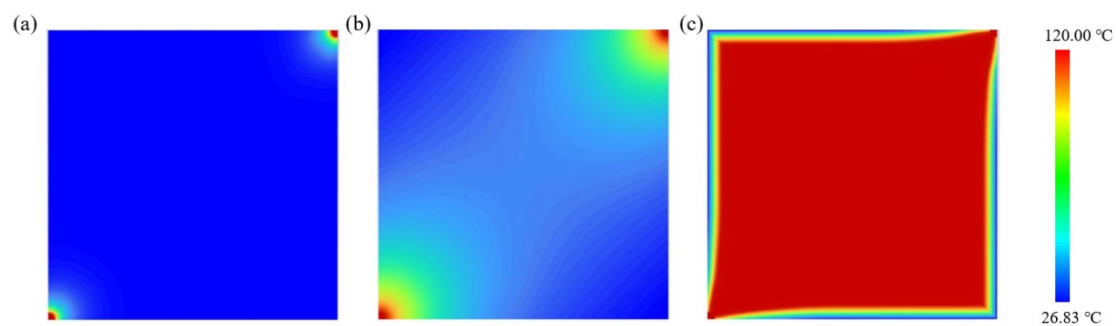


Figure S2. (a) ITO surface temperature distribution at the onset, (b) ITO surface temperature distribution after 0.1 s, (c) ITO surface temperature distribution after thermal stabilization.

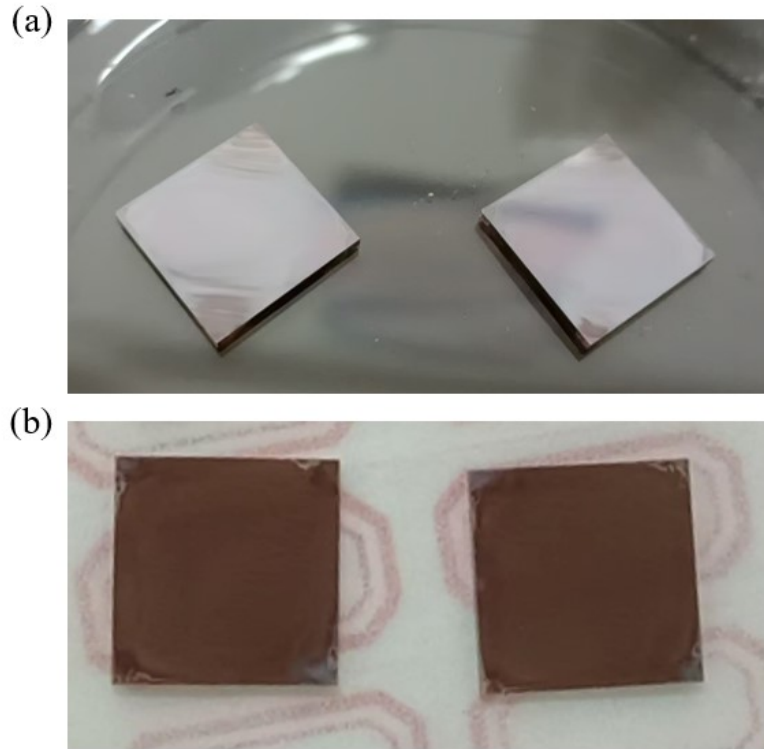


Figure S3. (a) Oblique Views of the surface of PCHM-Prepared Perovskite Solar Cells: the left shows a contact surface that is too large, and the right shows a moderate contact surface. (b) Top view of the dark brown CsPbI_2Br film under ambient conditions of dry air and room temperature after PCHM.

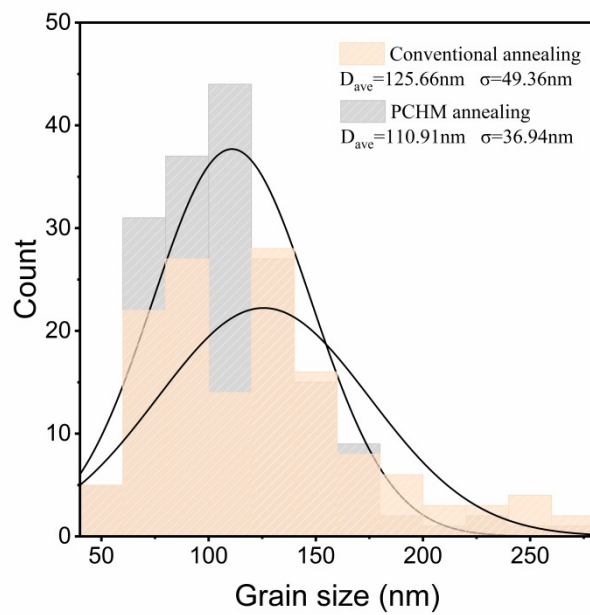


Figure S4. SEM Diagram of Grain Size Statistics for Conventional Heating and PCHMConventional two-step annealing and PCHM.

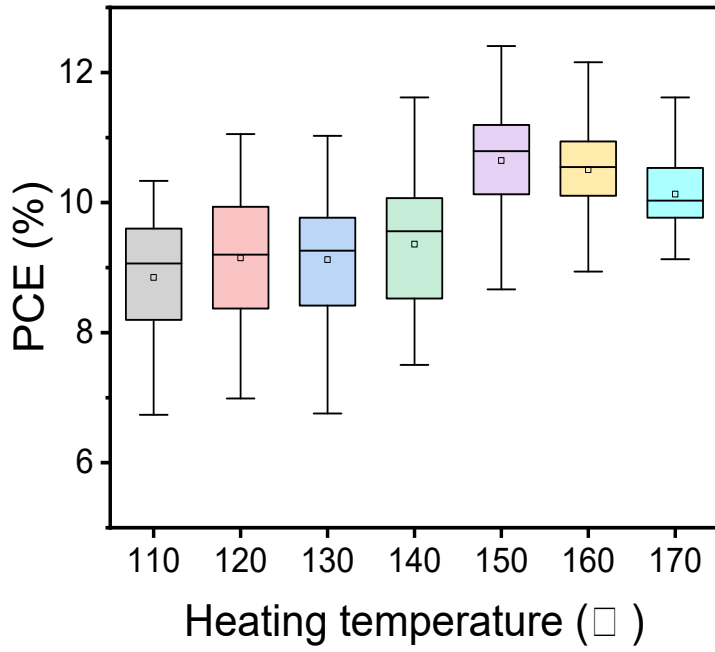


Figure S5. PCE box plots of the control device at different annealing temperatures based on PCHM method.

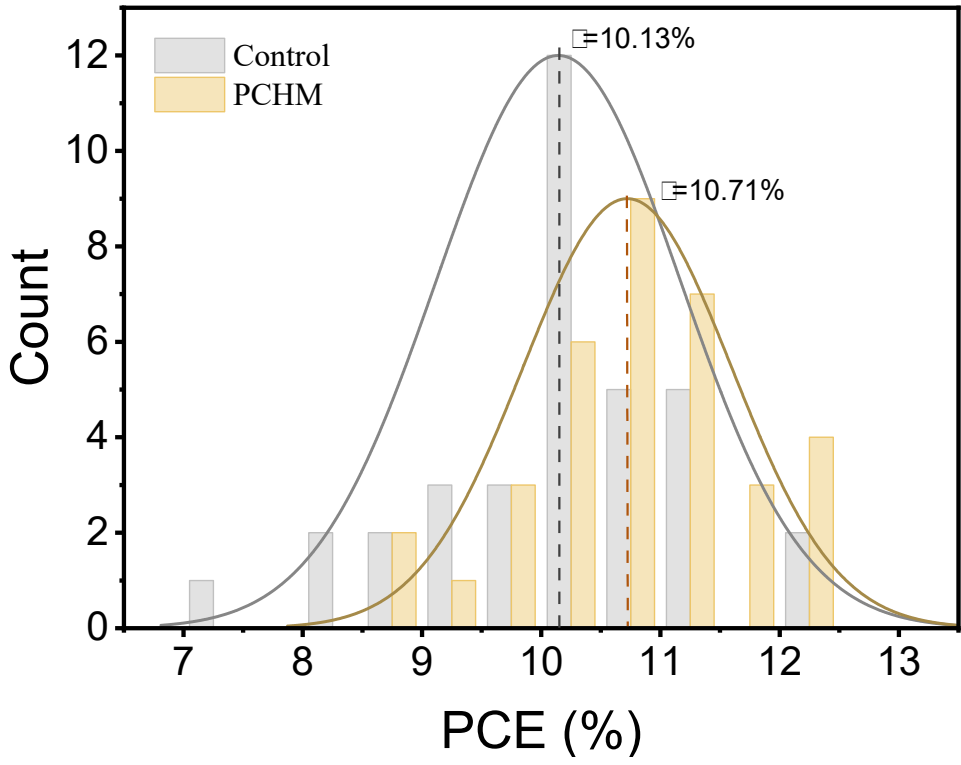


Figure S6. PCE statistics of conventional two-step heating method and PCHM.

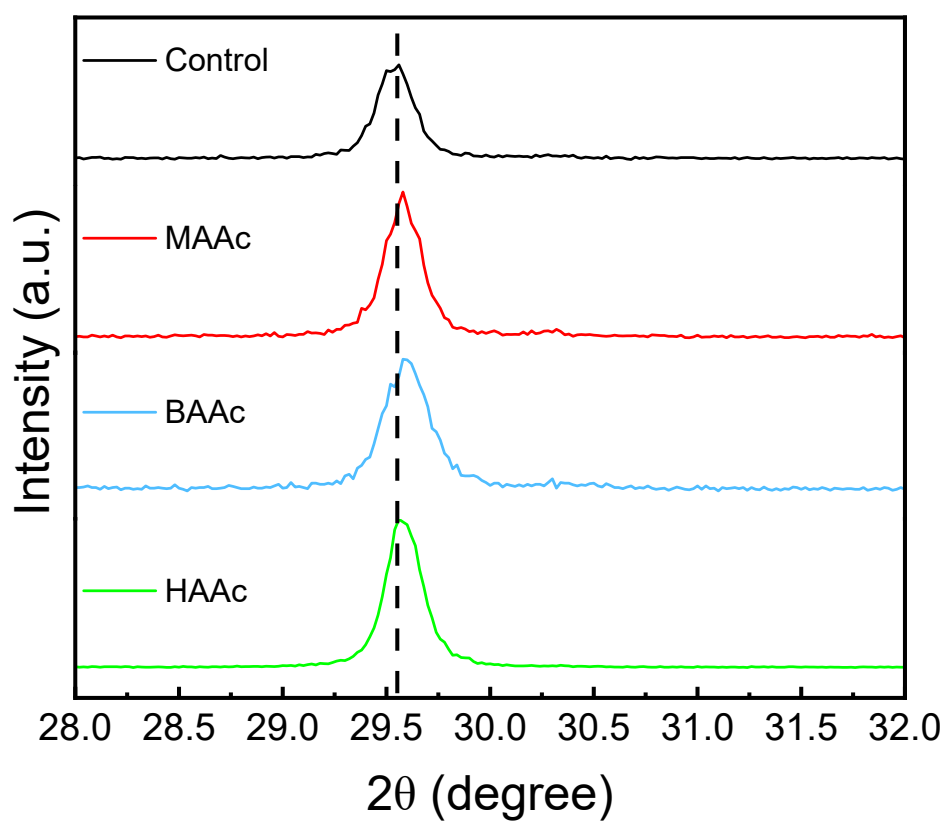


Figure S6. Partially enlarged views of the (200) XRD peaks.

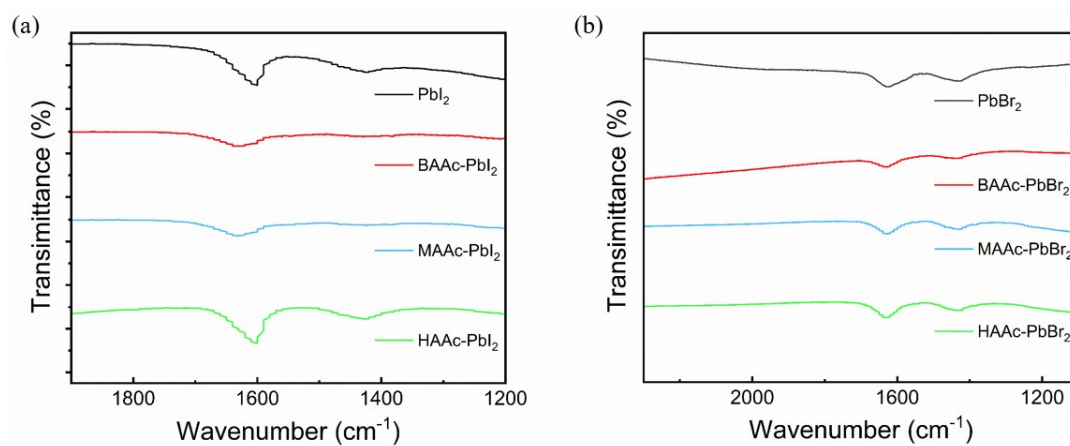


Figure S7. FTIR spectra: a) PbI_2 (powder) and PbI_2 -MAAC/BAAC/HAAC(film); b) PbBr_2 (powder) and PbBr_2 -MAAC/BAAC/HAAC(film). (the Treated: A mixture of PbI_2 and PbBr_2 with MAAC/BAAC/HAAC dissolves in a DMSO/DMF solvent and was then annealed to form a film)

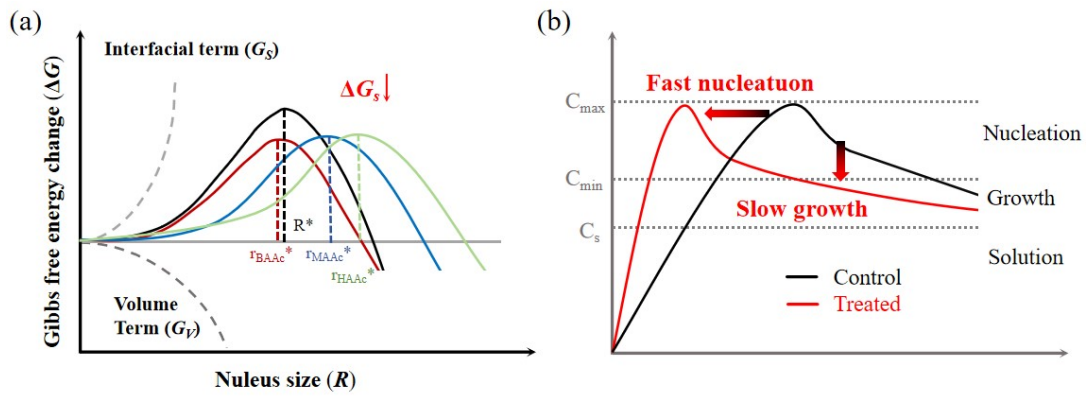


Figure S8. Schematic diagram of nucleation and crystallization. a) Gibbs energy and b) LaMer diagram for nucleation and crystallization dynamics of solution-processed crystals.

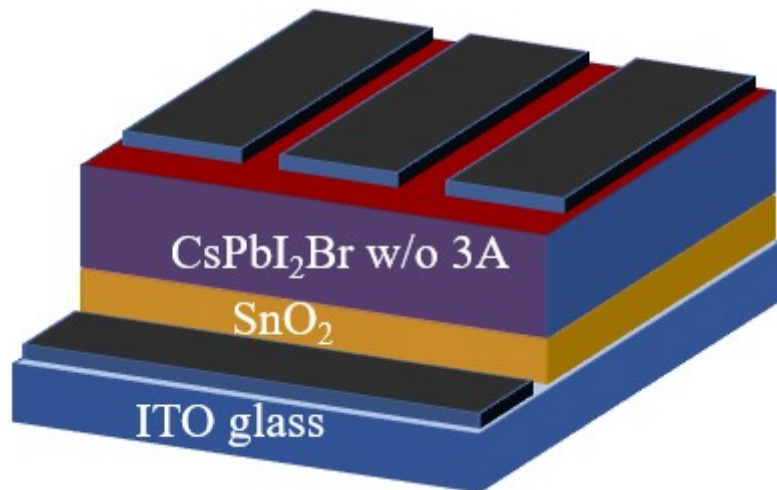


Figure S9. The device architecture: ITO/ SnO_2 / CsPbI_2Br (w/ or w 3A)/Carbon.

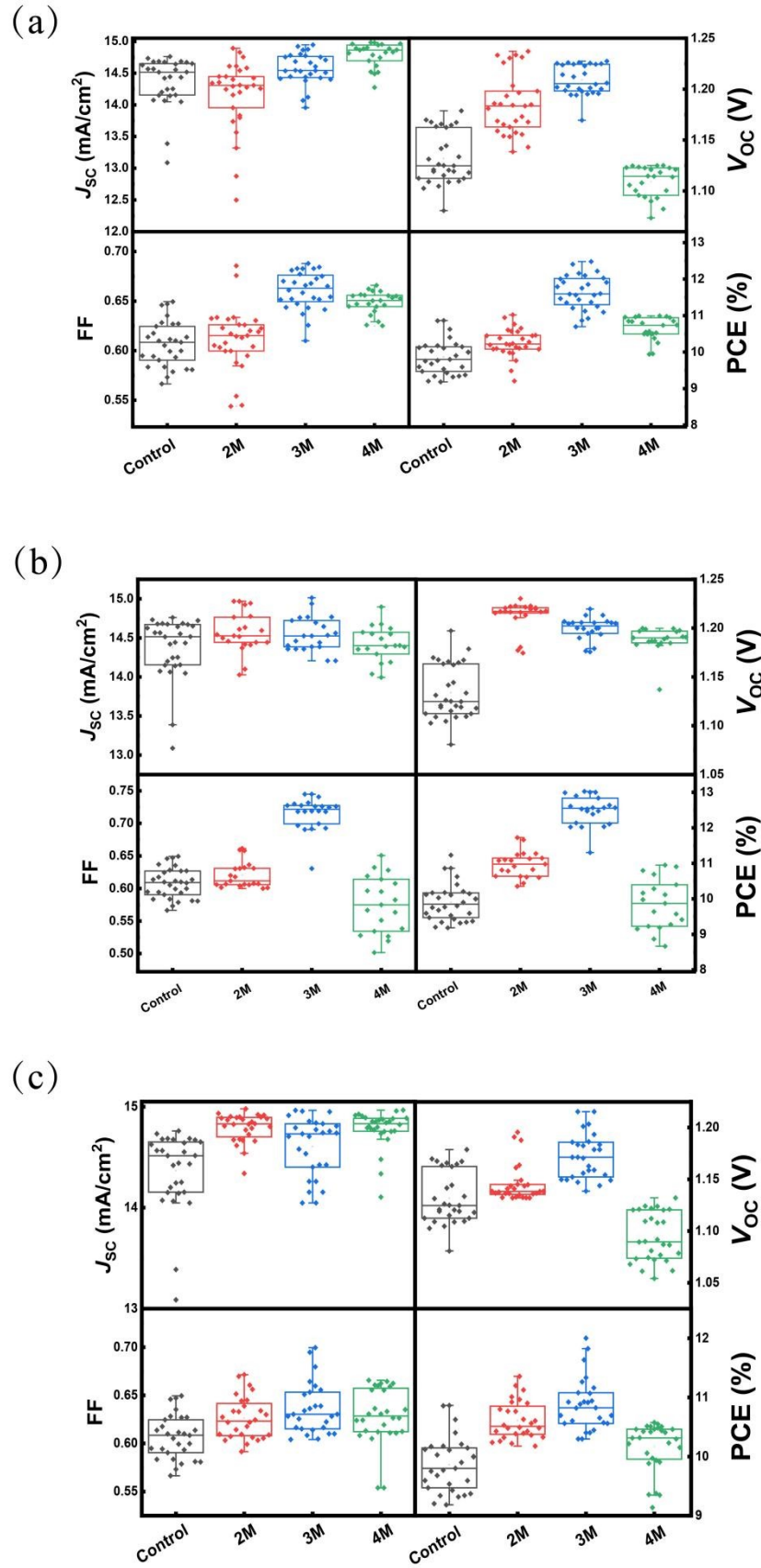


Figure S10. Box diagrams of photovoltaic parameters for 3A additives: (a) MAAC, (b) BAAC, (c) HAAC.

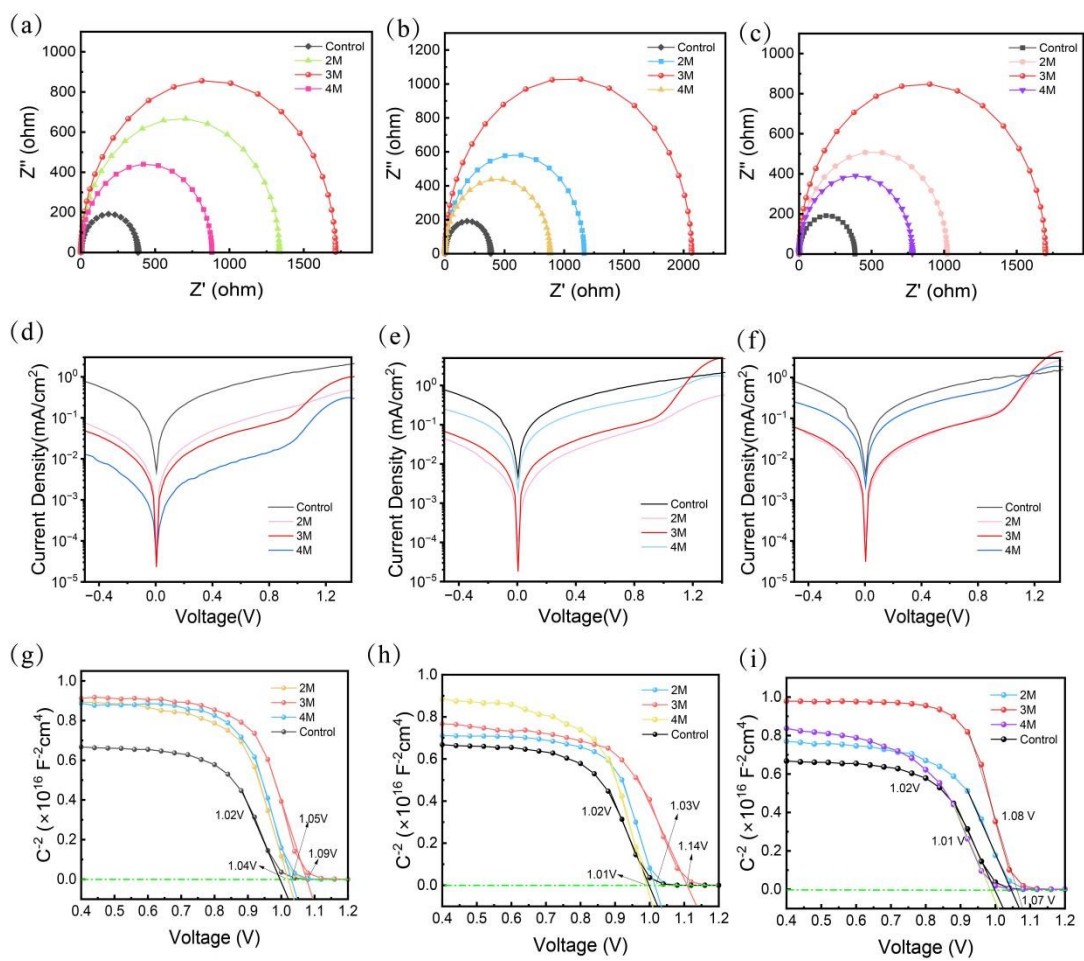


Figure S11. (a–c) Nyquist plots of different PSCs measured by EIS. (d–f) $J-V$ curves measured in the dark and (g–i) Mott–Schottky spectra of the PSCs containing, from left to right, MAAc, BAAC, and HAAC at different additive concentrations.

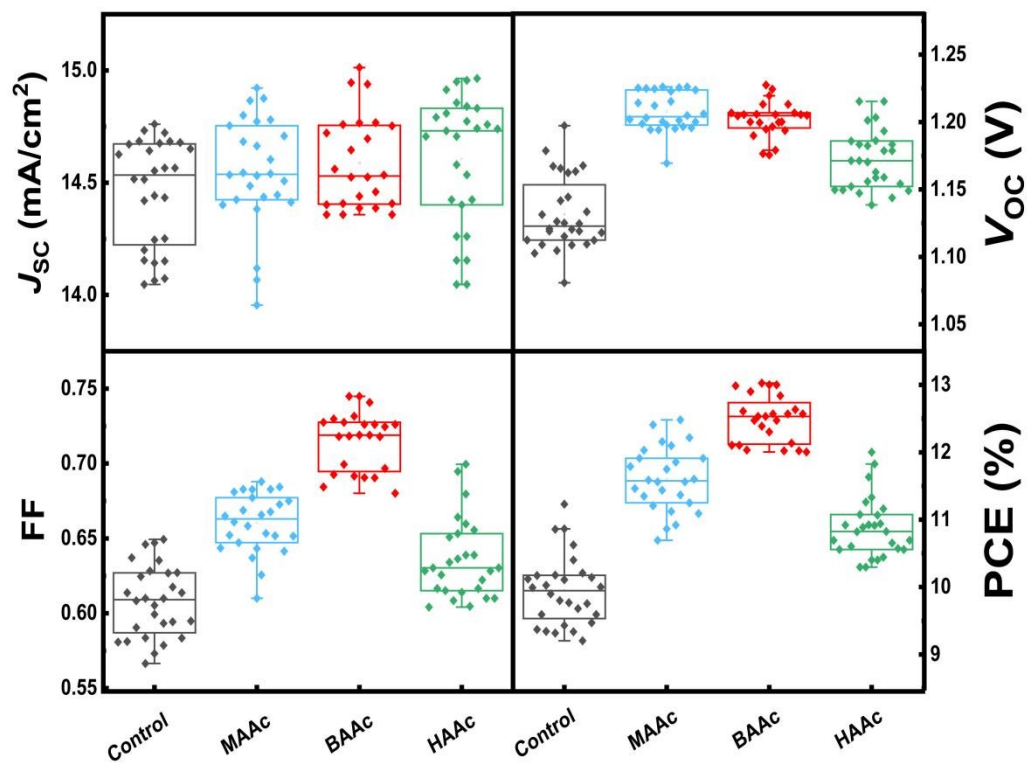


Figure S12. Box plots for the optimization of V_{OC} , J_{SC} , FF, and PCE.

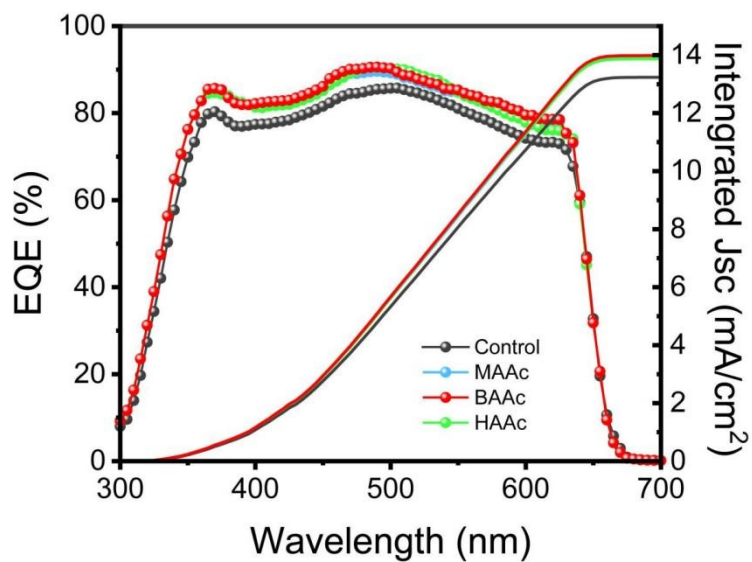


Figure S13. EQE spectra and integral currents

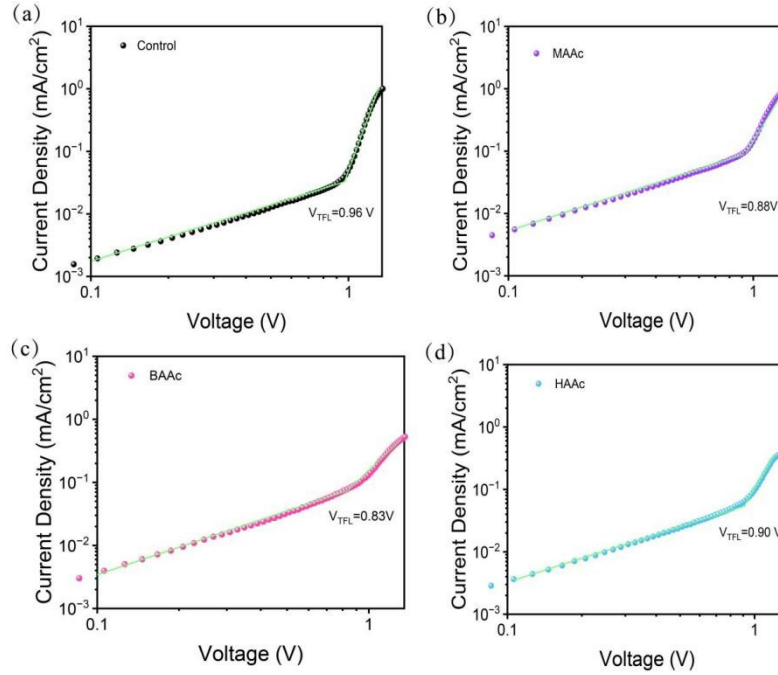


Figure S14. (a–d) The space-charge-limited-current (SCLC) model of PSCs without and with MAAc, BAAc, and HAAc additives.

2. Specification of reasons for changes in the annealing process

According to the previous studies of the two-step temperature-controlled method, we first focused on improving the annealing method to cope with the effect of the solvent volatilization mode on nucleation crystallization. In order to fabricate the highly crystalline and high-quality perovskite film, we have designed a simple annealing device as shown in **Figure 1a**.

In the past, the problem of nucleation size and uniformity due to the difference in solvent volatilization rates between the upper and lower surfaces is neglected. The overhead annealing method, which is heated at both ends, can completely avoid the above shortcomings. The new annealing method simply change the nucleation from the original full-domain intrinsic probabilistic nucleation to a local-ordered nucleation[4]. Therefore, it is generally assumed that their grain size distributions remain self-similar and the average growth rate of individual grain with radius r can be expressed as:

$$\frac{dr}{dt} \cong \frac{M\bar{\gamma}_{gb}}{2} \left(\frac{1}{r^*} - \frac{1}{r} \right)$$

where r^* is a critical radius found to be the average radius \bar{r} for two dimensional systems and \bar{r} for three-dimensional systems for which growth occurs with self-similar grain size distributions, $\bar{\gamma}_{gb}$ is the average grain boundary energy per unit area of grain boundary and M can be taken to be the average grain boundary mobility, which has the form (1). This growth rate equation incorporates the expectation that grains that are larger than the average grain size will grow, while grains that are smaller than the average size will tend to shrink and disappear[5, 6].

In addition to the changes in the annealing method allowing control of the nucleation size of crystalline grains, the growth rate equation and its continuity requirement emphasize that the modulation of the deterministic components of grain growth is critical for grain nucleation and crystallization. Previous modulation techniques commonly involve tedious and rigorous fabrication process, such as solvent and/or anti-solvent-assisted, and extended annealing time, to obtain perovskite films with highly ordered crystals and low defect states[7]. However, this existing fabrication methods hampers their suitability for fast and robust fabrications. Therefore, precursor engineering is a no-brainer for fabricating high-quality inorganic CsPbI₂Br perovskite film without increasing the complexity of preparation.

2.1 Supplementary formula:

The average grain boundary mobility, the expression is **form (1)**, show as:

$$M = M_0 \exp\left(\frac{-Q}{kT}\right)$$

M_0 is a weakly temperature-dependent constant and Q is the activation energy for the rate limiting atomic process required for grain boundary motion, and k and T have their usual meanings.

Whereas the continuity of grain fluxes in size space requires that :

$$\frac{\partial f(r,t)}{\partial t} = \frac{\partial}{\partial t} \left[f(r,t) \frac{dr}{dt} \right] + D \frac{\partial^2 f}{\partial r^2}$$

where $f(r, t)$ is the continuous distribution function that describes the number of

grains as a function of the grain sizes r , at a time t , D is a temperature-dependent but r -independent constant. where the first term on the right hand side represents a deterministic drift and the second term corresponds to a probabilistic diffusion.

3. Calculation section

3.1 TRPL decay spectrum

The TRPL decay spectrum is fitted by the bi-exponential function(**Equation S1**):

$$y(t) = A_1 e^{-t/\tau_1} + A_2 e^{-t/\tau_2} + y_0$$

where τ_1 and τ_2 are first- and second-order decay times, A_1 and A_2 represent weighting coefficients of each decay channel, y_0 is a constant.

The average carrier lifetime (τ_{pl}) can be estimated according to the **Equation S2**:

$$\tau_{ave} = \frac{A_1 \tau_1}{A_1 \tau_1 + A_2 \tau_2} \tau_1 + \frac{A_2 \tau_2}{A_1 \tau_1 + A_2 \tau_2} \tau_2$$

3.2 Dark J-V curve

The ideality factor (m) is obtained according to the **Equation S3**:

$$m = \frac{KT d \ln j}{q dV}$$

where K and T represent Boltzmann constant and absolute temperature, respectively.

3.3 TPV measurement

The TPV data are fitted and calculated according to the **Equations S1** and **S2**.

3.4 Trap state density

The SCLC model is applied to electron-only devices to quantitatively estimate trap state density (N_t) (**Equation S4**):

$$N_t = \frac{2\varepsilon_0 \varepsilon_r V_{TFL}}{qL^2}$$

where ε_0 is relative dielectric constant of CsPbI₂Br ($\varepsilon_r = 8.6$), V_{TFL} is trap-filling limit voltage, q is elementary charge and L is the thickness of CsPbI₂Br film.

3.5 Light intensity-dependent J-V measurement

The open-circuit voltage (V_{oc}) and short-circuit current density (J_{sc}) as a

function of light intensity (P_{light}) are fitted by **Equations S5** and **S6**, respectively:

$$V_{OC} = \frac{nKT}{q} \ln(P_{light}) + Constant$$

$$J_{SC} \propto P_{light}^{\alpha}$$

Where n is ideality, T is temperature, k is the Boltzmann constant and q is the elementary charge.

3.6 C-V measurement

The built-in potential (V_{bi}) can be calculated according to the **Equation S7**:

$$\frac{1}{C^2} = \frac{2(V_{bi} - V)}{A^2 q \epsilon_0 \epsilon_i N_A}$$

where N_A is carrier density.

3.7 DFT calculations

All calculations in this study were performed with the Materials Studio (MS) within the frame of density functional theory (DFT). Firstly, select the Forcite module for calculation. Secondly, under the Forcefield mode, specify COMPASSII as the force field. Thirdly, and configure the corresponding charge type to ensure accurate calculations. Finally, within the Forcite module, explicitly choose "Energy" as the calculation task for subsequent energy calculations. The lattice parameters and ionic position were fully relaxed, and the total energy was converged within 10^{-5} eV per formula unit. The final forces on all ions are less than 0.02 \AA^{-1} . The electrostatic potential (ϕ) was calculated using Gaussian 16W software with the B3LYP exchange-correlation functional.

Table S1. The binding energy of BAAC-PbI₂, MAAC-PbI₂ and HAAC-PbI₂ obtained from DFT calculation.

	PbI ₂	BAAC	MAAC	HAAC	BAAC+PbI ₂	MAAC+PbI ₂	HAAC+PbI ₂
Temperature (°C)	298.15	298.15	298.15	298.15	298.15	298.15	298.15
Pressure (atm)	1	1	1	1	1	1	1
EE (eV)	- 148.33	11,936. 02	8,748. 34	14,061 .07	-12,085.21	-8,897.45	-14,210.13
E _{int} (eV)					-0.86	-0.78	-0.73

$$E_{int} = E_{molecule-perovskite} - E_{perovskite} - E_{molecule}$$

Table S2. Parameters of the TRPL spectroscopy without and with MAAC, BAAC, and HAAC additives.

Device	A ₁	τ_1 (ns)	A ₂	τ_2 (ns)	τ_{ave} (ns)
Control	0.38	3.21	0.61	4.93	4.23
MAAC-treated	0.20	4.46	0.79	19.02	15.92
BAAC-treated	0.11	3.86	0.87	19.35	17.26
HAAC-treated	0.51	3.37	0.49	28.81	15.84

Table S3. Parameters for typical J - V characteristics of the device, including Voc, Jsc, FF, PCE, R_S and R_{rec}.

	V _{OC} (V)	J _{sc} (mA/cm ²)	FF	PCE (%)	R _S (Ω)	R _{rec} (Ω)
Control	1.11 V	14.62	61.63%	10.0%	10.56	384.71
MAAC	1.22 V	14.95	68.43%	12.48%	7.57	1682.35
BAAC	1.22	14.78	74.85%	13.50%	5.01	1716.96
HAAC	1.15 V	14.91	69.95%	12.0%	5.30	2063.06

Table S4. Parameters of the TPC spectroscopy without and with MAAC, BAAC, and HAAC additives.

Device	A ₁	τ_1 (μ s)	A ₂	τ_2 (μ s)	τ_{ave} (μ s)
Control	0.67	0.49	0.14	3.15	2.04
MAAC-treated	0.55	0.23	0.16	1.82	1.45
BAAC-treated	0.71	0.35	0.87	2.07	1.34
HAAC-treated	0.76	0.55	0.49	3.29	1.90

Table S5. Parameters of the TPV spectroscopy without and with MAAC, BAAC, and HAAC additives.

Device	A ₁	τ_1 (μ s)	A ₂	τ_2 (μ s)	τ_{ave} (μ s)
Control	0.26	55.8	0.72	181	175
MAAC-treated	0.37	39.8	0.65	469	637
BAAC-treated	0.35	89.6	0.61	679	449
HAAC-treated	0.39	18.7	0.62	222	199

The τ_{ave} is calculated by the Equation S2.

References

- [1] C. Liu, W. Li, C. Zhang, Y. Ma, J. Fan, Y. Mai, *J. Am. Chem. Soc.*, 2018, 140, 3825-3828.
- [2] C. Liu, W. Li, H. Li, H. Wang, C. Zhang, Y. Yang, X. Gao, Q. Xue, H. L. Yip, J. Fan, R. E. I. Schropp, Y. Mai, *Adv. Energy Mater.*, 2018, 9.
- [3] C. Liu, Y. Yang, C. Zhang, S. Wu, L. Wei, F. Guo, G. M. Arumugam, J. Hu, X. Liu, J. Lin, R. E. I. Schropp, Y. Mai, *Adv. Mater.*, 2020, 32.
- [4] C. V. Thompson, *Annu. rev. Mater.*, 1990, 20, 245-68.
- [5] K. J. Wu, E. C. M. Tse, C. Shang, Z. Guo, *Prog. Mater. Sci.*, 2022, 123.
- [6] M. Cai, P. Li, J. Ma, Y. Cheng, X. Xu, Z. Ren, Y. Song, *Nano Today*, 2024, 54.
- [7] J. Xue, R. Wang, K.-L. Wang, Z.-K. Wang, I. Yavuz, Y. Wang, Y. Yang, X. Gao, T. Huang, S. Nuryyeva, J. W. Lee, Y. Duan, L.-S. Liao, R. Kaner, Y. Yang, *J. Am. Chem. Soc.*, 2019, 141, 13948-13953.